INTERPOLATION FILTERS FOR ANTIDERIVATIVE ANTIALIASING

Victor Zheleznov and Stefan Bilbao

Acoustics and Audio Group
University of Edinburgh
Edinburgh, UK
victorzheleznov@ya.ru | s.bilbao@ed.ac.uk

ABSTRACT

Aliasing is an inherent problem in nonlinear digital audio processing which results in undesirable audible artefacts. Antiderivative antialiasing has proved to be an effective approach to mitigate aliasing distortion, and is based on continuous-time convolution of a linearly interpolated distorted signal with antialiasing filter kernels. However, the performance of this method is determined by the properties of interpolation filter. In this work, cubic interpolation kernels for antiderivative antialiasing are considered. For memoryless nonlinearities, aliasing reduction is improved employing cubic interpolation. For stateful systems, numerical simulation and stability analysis with respect to different interpolation kernels remain in favour of linear interpolation.

1. INTRODUCTION

Many systems of interest in virtual analog modelling, such as overdrive pedals, tube amplifiers, ladder filters, etc., include nonlinear components that produce harmonic distortion. Their simulation in discrete time at a standard sampling rate such as 44.1 kHz often leads to undesirable *aliasing* due to the bandwidth expansion of a signal beyond the Nyquist limit. The audibility of aliasing artefacts depends on the spectral content of the input signal and the nonlinearity itself.

The most common way of dealing with aliasing is *oversampling*: the desired system is simulated at a higher sampling rate and a digital low-pass filter is employed in series to remove frequency components above the Nyquist limit before returning to the original sampling rate. While oversampling has proved to be effective [1], the computational load can rise significantly since it is proportional to the oversampling factor [2].

For memoryless nonlinearities, an alternative approach has been proposed called *antiderivative antialiasing* (AA) [3]. In this approach, linear interpolation is employed to construct a continuous-time signal, and then applying a nonlinear function and a finite impulse response (FIR) low-pass filter in a continuous-time domain. Since there is a linear relationship between time and signal amplitude, it is possible to formulate an analytical discrete-time solution in terms of antiderivative of the nonlinear function by integrating out the continuous-time variable. AA has proved to be more efficient than oversampling and can be generalised to higher orders [2]. This method was extended to include arbitrary order infinite impulse response (IIR) filters [4], thus improving capabilities of continuous-time antialiasing filters. The original AA method and its extension to IIR filters will be referred to as AA-FIR and AA-IIR, respectively. The AA structure is summarised in fig. 1.

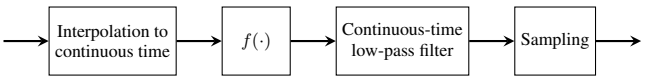

Figure 1: *AA for a memoryless nonlinearity* $f(\cdot)$.

For stateful systems, the AA-FIR method was applied [5, 6] and showed significant improvements without increasing the computational cost for state-space models with a scalar nonlinearity [7]. Since the FIR filters employed are linear phase and introduce constant delay for all frequencies, this delay can be compensated for by designing a stateful system at a reduced sampling rate to avoid instability. In contrast, IIR filters are known to have a nonlinear phase response, and thus a frequency compensation approach was proposed to employ the AA-IIR method inside a stateful system [8]. It adds a digital compensation filter in series for each antialiased nonlinearity to compensate for the phase distortion and frequency-dependent effects introduced by the AA-IIR method.

All currently proposed AA methods use linear interpolation to construct a continuous-time signal. However, it has been shown that for higher order low-pass filters the AA-IIR method attains the upper performance bound imposed by linear interpolation [4]. This suggests that aliasing reduction can be improved if better interpolation kernels, in terms of better attenuation in the stopband, are used to construct a continuous-time signal. More crucially, the stability of the extension of the AA-IIR method to stateful systems depends both on interpolation and antialiasing filters. The initial study of this extension [8] concluded that only first order low-pass filters can be used in combination with linear interpolation, which poses a severe limitation on the AA-IIR method. In this work, we consider the use of cubic interpolation kernels for the AA-IIR method, and investigate through numerical simulation how this affects aliasing reduction and stability conditions of the method.

The paper is organised as follows. Cubic interpolation kernels are defined in Section 2, and the AA-IIR method for memoryless and stateful systems is summarised in Section 3. In Section 4, stability conditions for the digital compensation filter are studied, expanding the work by La Pastina et al. [8]. Section 5 is devoted to the implementation of cubic AA-IIR and its evaluation against oversampling and linear AA-IIR for several test systems.

2. CUBIC INTERPOLATION

Consider a sequence of samples $x[n]$ which originates from uniform sampling of a signal $x(t)$ at times $t = nT,\ n \in \mathbb{N}$. For simplicity, the unit sampling interval $T = 1$ is assumed without loss of generality.

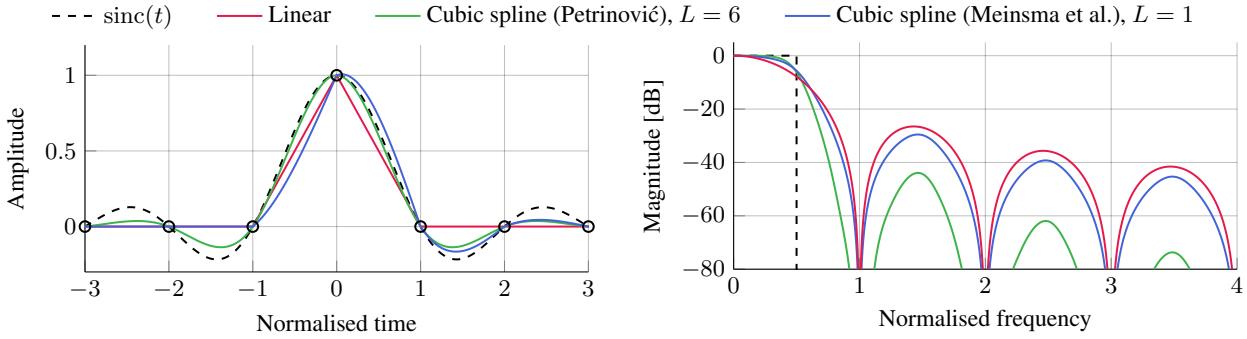

(a) Interpolation kernels $\varphi_{\text{int}}(\cdot)$.

(b) Spectrum of interpolation kernels.

Figure 2: *Piecewise polynomial interpolation.*

An interpolated value $\widetilde{x}(t)$ at some time t can be expressed as a sample-weighted sum of integer shifts of an interpolation kernel $\varphi_{\text{int}}(\cdot)$:

$$\widetilde{x}(t) = \sum_{n\in\mathbb{Z}} x[n]\varphi_{\text{int}}(t-n), \tag{1}$$

where $\varphi_{\text{int}}(0) = 1$ and $\varphi_{\text{int}}(n) = 0,\ \forall n \in \mathbb{Z},\ n \neq 0$. For a piecewise polynomial kernel of degree d, we can rewrite (1) as:

$$\widetilde{x}(t)|_{t\in[n,n+1]} = \sum_{i=0}^{d} c_i[n](t-n)^i =: P_n(t-n),$$

where $c_i[n]$ are coefficients of an interpolating polynomial $P_n(\cdot)$.

To allow for an extended choice of kernels, the interpolation process can be decomposed into two stages [9] and represented by a filtering procedure in z-domain in fig. 3 [10]. Firstly, interpolation coefficients $\boldsymbol{w}[n]$ are obtained by applying a pre-filter with a transfer function $\boldsymbol{H}(z)$ to the signal samples $x[n]$. Secondly, an output filter $\boldsymbol{G}(z)$ is used to obtain polynomial coefficients $\boldsymbol{c}[n]$.

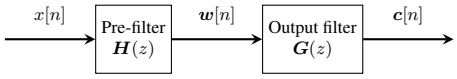

Figure 3: *General structure of piecewise polynomial interpolation.*

Properties of an interpolation kernel $\varphi_{\text{int}}(\cdot)$ can be compared to the ideal reconstruction kernel $\text{sinc}(\cdot)$. In particular, cubic splines represent an efficient way to approximate this ideal reconstruction [11]. Numerous approaches to construct splines with desired smoothness properties are available in the literature [12, 13]. However, they are non-causal interpolators, and for real-time audio processing this issue needs to be addressed. For memoryless nonlinearities, some processing latency is acceptable, thus allowing interpolation filters with a finite look-ahead of future signal samples. For stateful systems, only strictly causal interpolation algorithms can be considered due to the embedded feedback loops.

2.1. Causal Spline Formulation by Petrinović

The non-causal cubic spline pre-filter can be represented in the following cascade implementation [13]:

$$H_{\text{nc}}(z) = \frac{1}{z+4+z^{-1}} = \underbrace{\frac{-\gamma}{1-\gamma z^{-1}}}_{H_+(z)}\underbrace{\frac{1}{1-\gamma z}}_{H_-(z)},$$

where $\gamma = \sqrt{3}-2$. One way to address the causality issue is to truncate the anti-causal part $H_-(z)$ of the cubic spline pre-filter, thus allowing a finite look-ahead of $L_H \geq 1$ samples:

$$H_{\text{cas}}(z) = H_+(z)\left(1+\sum_{k=1}^{L_H}\gamma^k z^k\right).$$

Causal spline formulations that arise from truncation of the pre-filter $H_{\text{nc}}(z)$ were explored by Petrinović [10, 11]. It was shown that the cascade implementation $H_{\text{cas}}(z)$, combined with an output filter $\boldsymbol{G}(z)$ based on de Boor's matrix representation of spline [12], compared favourably in terms of computational cost and performance to other formulations. The closed-form solution is expressed as:

$$\boldsymbol{H}(z) = \begin{bmatrix} H_{\text{cas}}(z) \\ 1 \end{bmatrix},$$

$$\boldsymbol{G}(z) = \begin{bmatrix} 0 & 1 \\ 3(z-z^{-1}) & 0 \\ -3(z^2+2z-1-2z^{-1}) & 3(z-1) \\ 3(z^2+z-1-z^{-1}) & -2(z-1) \end{bmatrix}. \tag{2}$$

As seen from (2), the output filter $\boldsymbol{G}(z)$ has a fixed look-ahead $L_G = 2$. The overall look-ahead for the outlined causal spline formulation is $L = L_H + L_G \geq 3$. Thus, this formulation is only suitable for memoryless nonlinearities. For a common oversampling factor $M = 8$, the look-ahead of $L = 6$ would be enough to achieve approximately the same interpolation accuracy as the non-causal cubic spline [10].

2.2. Causal Spline Formulation by Meinsma et al.

In the works by Meinsma et al. [14, 15] signal interpolation process is explored from a system-theoretic point of view. Authors pose a mean-square optimisation problem on the combined sampling and reconstruction system with a causality constraint. For uniform sampling, an optimal closed-form solution to the signal reconstruction problem in terms of reconstruction error is derived for an arbitrary look-ahead L, including $L = 1$ suitable for application in stateful systems. In such a case, the closed-form solution

is represented in the following way [16]:

$$\boldsymbol{H}(z) = \begin{bmatrix} 4 - \sqrt{3} + \frac{6\gamma}{z-\gamma} \\ 3 - \sqrt{3} + \frac{6\gamma}{z-\gamma} \\ -6\gamma\frac{(z-1)^2}{z-\gamma} \\ 0 \end{bmatrix},$$

$$\boldsymbol{G}(z) = \begin{bmatrix} 1 & -1 & 0 & 0 \\ 0 & 1 & \frac{1}{2\sqrt{3}} & \frac{1}{2\sqrt{3}} \\ 0 & 0 & \frac{1}{2} & \frac{1}{2} \\ 0 & 0 & -\frac{1}{6} & 0 \end{bmatrix}.$$

However, for an equal look-ahead the Petrinović formulation is more computationally efficient [16]. The comparison between chosen cubic interpolation kernels is shown in fig. 2. All of the cubic interpolation kernels compare favourably to linear interpolation in both the passband and the stopband.

3. ANTIDERIVATIVE ANTIALIASING WITH INFINITE IMPULSE RESPONSE FILTERS

3.1. Memoryless Nonlinearities

After constructing a continuous-time signal $\widetilde{x}(\cdot)$, the AA-IIR method solves a continuous-time convolution of the nonlinearly processed signal $f(\widetilde{x}(\cdot))$ with an IIR low-pass filter kernel (see fig. 1). In particular, the AA-IIR method utilises IIR filters with a rational Laplace transfer function $H(s) = \frac{F(s)}{G(s)}$, where $F(s)$ and $G(s)$ are real-valued polynomials with $\deg F \leq \deg G$ [4]. Such a function can be expanded using partial fraction decomposition:

$$H(s) = A_0 + \sum_{k=1}^{p}\sum_{l=1}^{m_k} \frac{A_{kl}}{(s-\alpha_k)^l} + \\ + \sum_{k=1}^{q}\sum_{l=1}^{\mu_k}\left(\frac{B_{kl}}{(s-\beta_k)^l} + \frac{\overline{B}_{kl}}{(s-\overline{\beta}_k)^l}\right), \quad (3)$$

where $\alpha_1, \ldots, \alpha_p$ are real poles with multiplicities $m_1, \ldots, m_p$ and $\beta_1, \ldots, \beta_q$ are complex poles with multiplicities $\mu_1, \ldots, \mu_q$. Since the transfer function is assumed to be real-valued, each complex pole β_k has a complex conjugate pair $\overline{\beta}_k$.

The result of filtering a continuous-time signal $f(\widetilde{x}(\cdot))$ by an IIR filter with the transfer function $H(s)$ can be obtained by treating each summand in (3) separately and combining their outputs.

3.1.1. Distinct Pole

Suppose that $H(s)$ has only a single distinct pole $\alpha \in \mathbb{R},\ \alpha < 0$, meaning $H(s) = \frac{A}{s-\alpha},\ A \in \mathbb{R}$. The inverse Laplace transform of $H(s)$ takes the form $h(t) = Ae^{\alpha t}\vartheta(t)$, where $\vartheta(t)$ is the Heaviside step function. For the AA-IIR output $y[n]$ we get the following recursive expression [8]:

$$y[n] = \int_0^n f(\widetilde{x}(t))h(n-t)\,dt = \\ = e^{\alpha}y[n-1] + A\int_0^1 f(\widetilde{x}(n-1+t))e^{\alpha(1-t)}\,dt. \quad (4)$$

For linear interpolation, closed-form solutions to the convolution integral in (4) are possible, but would depend on the nonlinearity $f(\cdot)$, unlike in the AA-FIR method. For cubic interpolation only numerical solutions are possible since the integral, except for polynomial nonlinearity, would be nonelementary.

3.1.2. Repeated Pole

For a repeated pole, meaning a pole with multiplicity value larger than one, the situation is more complex. Suppose that $H(s) = \frac{A}{(s-\alpha)^{r+1}},\ r \in \mathbb{N},\ \alpha \in \mathbb{R},\ A \in \mathbb{R}$ with $\alpha < 0$. The inverse Laplace transform of $H(s)$ takes the form $h(t) = A\frac{t^r}{r!}e^{\alpha t}\vartheta(t)$. After applying the binomial expansion inside the convolution integral, we obtain the following AA-IIR expression [8]:

$$y[n] = \frac{1}{r!}u_r[n], \quad (5)$$

$$u_k[n] = e^{\alpha}\sum_{l=0}^{k}\binom{k}{l}u_l[n-1] + \\ + A\int_0^1 f(\widetilde{x}(n-1+t))(1-t)^k e^{\alpha(1-t)}\,dt, \quad (6)$$

$$k = 0, \ldots, r,$$

where we refer to $u_k[n]$ as the states of the AA-IIR method.

For both distinct and repeated poles, each complex conjugate pair of poles $\beta, \overline{\beta} \in \mathbb{C}$ is treated like a real pole with twice the residual value, and a real part of the AA-IIR output is taken. It is possible to derive a purely real two-step update for $y[n]$ [4], but this would increase computational cost [16].

3.2. Stateful Systems

Any AA method introduces delay and frequency-dependent effects due to the embedded filtering procedure. To implement the AA-IIR method inside a stateful system, a digital compensation filter is designed and added in series for each antialiased nonlinearity to mitigate these effects and ensure stability of the simulation [8]. Consequently, this filter needs to be an inverse of transfer function $H_{\text{lin}}(z)$ corresponding to linearisation of the AA-IIR method. Even though the compensation filter is applied in the end, thus affecting all spectral components including aliases, we expect that the antialiasing filter would attenuate them enough beforehand. The frequency compensation structure is presented in fig. 4.

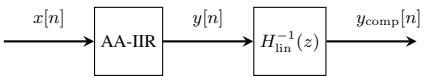

Figure 4: *Frequency compensation for the AA-IIR method.*

The overall linearisation $H_{\text{lin}}(z)$ of the AA-IIR method is computed as a sum of linearisation transfer functions for each pole of an IIR filter. To build up the compensation filter for any IIR filter with a rational transfer function, we first need to derive linearisation expressions for distinct and repeated poles.

3.2.1. Distinct Pole

Assume that $f(\cdot)$ is differentiable at 0 and $f(0) = 0$. For an interpolating polynomial $P_{n-1}(\cdot)$ of degree d between samples

$x[n-1]$ and $x[n]$, we get the following linearisation of the AA-IIR output equation (4) for a distinct pole $\alpha \in \mathbb{R}$:

$$\begin{aligned} y[n] - e^{\alpha} y[n-1] &= A \int_0^1 f(P_{n-1}(t)) e^{\alpha(1-t)}\, dt \approx \\ &\approx f'(0) A \int_0^1 P_{n-1}(t) e^{\alpha(1-t)}\, dt = \\ &= f'(0) \sum_{i=0}^{d} c_i[n-1] \underbrace{A \int_0^1 t^i e^{\alpha(1-t)}\, dt}_{S_i}. \end{aligned}$$

Taking z-transform on both sides of the equation, we obtain:

$$\begin{aligned} \widehat{Y}(z) &= f'(0) H_{\mathrm{lin}}(z) X(z), \\ H_{\mathrm{lin}}(z) &= \frac{\sum_{i=0}^{d} z^{-1} H_{C_i}(z) S_i}{1 - e^{\alpha} z^{-1}}, \end{aligned} \tag{7}$$

where $H_{C_i}(z) = \sum_j G_{ij}(z) H_j(z)$ is the combined transfer function of interpolation pre-filter and corresponding output filter for each polynomial coefficient and $\widehat{Y}(z)$ is the z-transform of output samples $\widehat{y}[n]$ obtained from linearisation.

3.2.2. Repeated Pole

For a repeated pole $\alpha \in \mathbb{R}$ with multiplicity $r+1,\ r > 0$, linearisation of the AA-IIR state update equation (6) is:

$$\begin{aligned} u_k[n] - e^{\alpha} \sum_{l=0}^{k} \binom{k}{l} u_l[n-1] \approx \\ f'(0) \sum_{i=0}^{d} c_i[n-1] \underbrace{A \int_0^1 t^i (1-t)^k e^{\alpha(1-t)}\, dt}_{S_{ik}}. \end{aligned} \tag{8}$$

Defining $\boldsymbol{u}[n] = \big(u_0[n], \ldots, u_r[n]\big)^{\mathrm{T}}$, $\boldsymbol{S}_i = \big(S_{i0}, \ldots, S_{ir}\big)^{\mathrm{T}}$ and a matrix $\boldsymbol{M}$ of binomial coefficients where $M_{ij} = \binom{i}{j},\ i \geq j$ and $M_{ij} = 0,\ i < j$, we can write the z-transform of the equation (8) in the following way:

$$\begin{aligned} \widehat{\boldsymbol{U}}(z) &= f'(0) \boldsymbol{H}_{\mathrm{lin}}(z) X(z), \\ \boldsymbol{H}_{\mathrm{lin}}(z) &= \big(\boldsymbol{I} - e^{\alpha} \boldsymbol{M} z^{-1}\big)^{-1} \left(\sum_{i=0}^{d} z^{-1} H_{C_i}(z) \boldsymbol{S}_i \right), \end{aligned}$$

where $\widehat{\boldsymbol{U}}(z)$ is the z-transform of states $\widehat{\boldsymbol{u}}[n]$ obtained from linearisation. Because only the last element of the vector $\boldsymbol{H}_{\mathrm{lin}}(z)$ corresponds to the AA-IIR output $y[n]$ (5), all of the other elements can be discarded.

4. STABILITY ANALYSIS OF COMPENSATION FILTER

To apply the AA-IIR method inside a stateful system, we need to understand which combinations of interpolation and antialiasing filters would result in a minimum-phase AA-IIR linearisation, leading to a stable simulation. Here we summarise some theoretical results to the AA-IIR linearisation, and numerically investigate stability of the compensation filter with regards to different interpolation and antialiasing filters.

4.1. Closed-Form Linearisation

The study by La Pastina et al. [8] derived closed-form linearised expressions for the linear AA-IIR method for the cases of a single distinct real pole, a single real pole with multiplicity of two and a single pair of distinct complex conjugate poles. In the case of a single distinct real pole it was analytically shown that linearisation is minimum-phase for any pole value $\alpha < 0$, while in other cases analytical minimum-phase analysis was not possible.

In addition, this study demonstrated that when employing nearest neighbour interpolation, restrictions on pole values in terms of stability of the compensation filter are relaxed compared to linear interpolation. However, for any type of piecewise constant interpolation the AA-IIR method results in a linear system with respect to function values $f(x[n])$. The compensation filter becomes equal to the exact inverse of the AA-IIR method and outputs $y_{\mathrm{comp}}[n] = f(x[n])$. This fact makes such interpolation of no practical use.

For cubic interpolation, the strictly causal spline in the formulation of Meinsma et al. is suitable for implementation inside a stateful system. In this case the linearised transfer function for a single distinct pole $\alpha \in \mathbb{R}$ can be derived from (7) and takes the following form:

$$\begin{aligned} H_{\mathrm{lin}}(z) &= A \frac{b_0 + b_1 z^{-1} + b_2 z^{-2}}{(1 - e^{\alpha} z^{-1})(1 - \gamma z^{-1})}, \\ b_0 &= \frac{\gamma}{\alpha^4} \Big[e^{\alpha} \big(6 - 6\alpha - \sqrt{3}\alpha^2\big) - 6 + \big(3 + \sqrt{3}\big)\alpha^2 + \\ &\quad + \big(2 + \sqrt{3}\big)\alpha^3 \Big], \\ b_1 &= \frac{\gamma}{\alpha^4} \Big[e^{\alpha} \big(-12 + 12\alpha + (\sqrt{3} - 3)\alpha^2 - \\ &\quad - (\sqrt{3} + 2)\alpha^3\big) + 12 - (\sqrt{3} + 3)\alpha^2 + \alpha^3 \Big], \\ b_2 &= \frac{\gamma}{\alpha^4} \Big[e^{\alpha} \big(6 - 6\alpha + 3\alpha^2 - \alpha^3\big) - 6 \Big], \end{aligned} \tag{9}$$

where $\gamma = \sqrt{3} - 2$. Zeros of the transfer function (9) can be derived analytically, but there is no way of determining for which pole values they are inside the unit circle.

4.2. Numerical Analysis

As we see from the results above, analytical minimum-phase analysis of the AA-IIR linearisation is limited. However, for fixed interpolation and antialiasing filter models, we can numerically check zeros of the AA-IIR linearisation while altering pole values of the antialiasing filter to approximate the stability region of the AA-IIR method. For completeness, numerical analysis was also carried out for piecewise constant interpolation kernels.

4.2.1. Real Pole

Consider the transfer function $H(s) = \frac{1}{(s-\alpha)^{r+1}}$ for a real pole $\alpha < 0$ with multiplicity $r+1,\ r \geq 0$. Results of numerical simulation for different interpolation kernels and multiplicity values using a step 10^{-2} for pole values $\alpha \in [-15, 0]$ are shown in

table 1. For all cases the maximum pole value $\alpha_{\max}$ was found so that we need to chose $\alpha < \alpha_{\max}$ to obtain a minimum-phase linearisation.

As evident from the table, higher-order interpolation kernels have more severe limitations on pole values α. For example, for linear interpolation there are no limitations on a distinct pole value, while for cubic interpolation we obtain $\alpha_{\max} = -2.05$ which might be too restrictive for practical applications. With increasing multiplicity r we also observe that the minimum-phase condition becomes more strict.

Table 1: *Upper bound $\alpha_{\max}$ for real pole values α for AA-IIR with different interpolation kernels.*

Interpolation	$r = 0$	$r = 1$	$r = 2$	$r = 3$
Next neighbour	0	0	-1.83	-3.16
Nearest neighbour	0	-3.01	-5.22	-7.29
Linear	0	-3.21	-5.54	-7.70
Cubic spline	-2.05	-5.92	-9.38	-12.77

4.2.2. Filter Designs

For common IIR filter designs such as Butterworth and Chebyshev filters numerical simulation was carried out for normalised cutoff values $f_c \in [0, 1]$ with a step 10^{-3} while fixing filter order and other parameters if necessary. Please note that for normalised sampling rate $f_s = 1$ the Nyquist limit corresponds to 0.5, and we should choose cutoff values around Nyquist to achieve sufficient aliasing reduction. Stability analysis of first order filters is omitted since it directly follows the case of a distinct real pole.

For the Butterworth filter of orders $K = 2, 3, 4$ we obtain a minimum stable cutoff frequency $f_c^{\min}$ so that we need to select $f_c \geq f_c^{\min}$ to satisfy stability of the compensation filter (see table 2). We observe that the only possibly practical combination is a second-order filter with linear interpolation since the restriction $f_c^{\min} = 0.507$ is close to the Nyquist limit.

For Chebyshev type II filter design we have a stopband attenuation parameter R_s. It was discovered that the stability region with decreasing R_s is no longer represented as a simply connected interval, but rather several different intervals combined. Taking linear interpolation as an example, for a second-order filter we get stability regions in table 3. The observed restrictions on the cutoff frequency are too harsh since we either are too far from the Nyquist limit or have a zero of the filter below the Nyquist limit. The latter would result in a sharp peak of the compensation filter for midrange frequencies which would amplify aliased components. Similarly, the use of Chebyshev type I and elliptic filters is not desired due to the passband ripple, since it would result in low and midrange frequency boosts in the compensation filter.

Table 2: *Lower bound $f_c^{\min}$ for cutoff frequency of Butterworth filter for AA-IIR with different interpolation kernels (dashes indicate bounds larger than one).*

Interpolation	$K = 2$	$K = 3$	$K = 4$
Next neighbour	0	0.357	0.501
Nearest neighbour	0.487	0.698	0.878
Linear	0.507	0.712	0.88
Cubic spline	0.793	—	—

Table 3: *Stability regions for cutoff frequency of Chebyshev type II filter with different values of stopband attenuation R_s for linear AA-IIR.*

R_s	$K = 2$
30 dB	$[0.001, 0.391]$
20 dB	$[0.001, 0.394]$
10 dB	$[0.001, 0.408] \cup [0.587, 1]$

5. CASE STUDIES

5.1. Metrics

Performance of algorithms was assessed on input sine tones across MIDI notes, ranging from the middle C note (261.63 Hz) to the top of MIDI range (G#9, 13289.75 Hz). For the signal quality evaluation signal-to-noise ratio (SNR) and noise-to-mask ratio (NMR) were considered.

SNR is an energy ratio between desired and aliased components in a signal. SNR is a widespread quality measure found in many works devoted to AA [3, 7], but it does not generally correlate to the perception of aliasing [1]. Compared to SNR, NMR takes into account frequency-dependent sensitivity of hearing and perceptual masking in the frequency domain. NMR is defined as an energy ratio between aliased components and the simplified masking threshold of desired components in a signal [17]. Since algorithms are evaluated on stationary signals, temporal masking is not considered. Signals with an NMR value below -10 dB are deemed to have inaudible aliasing [1].

To evaluate both SNR and NMR, the bandlimited signal containing only desired frequency components needs to be constructed. A one second fragment of the distorted signal is windowed by a Chebyshev window with 120 dB relative sidelobe attenuation [1]. Magnitude and phase values at integer multiples of fundamental frequency are obtained from the spectrum to additively synthesise the bandlimited signal. The aliased signal is constructed by subtraction of the bandlimited signal from the distorted signal.

5.2. Hard Clipper

The first case study is the hard clipping nonlinearity:

$$f(x) = \begin{cases} x, & |x| \leq 1; \\ \operatorname{sgn}(x), & |x| > 1. \end{cases}$$

Oversampling (OS) with a factor $M = 8$ is chosen as a baseline algorithm. We utilise an 8th order Chebyshev type I filter for decimation with passband ripple 0.05 dB and cutoff at $0.4 f_s$ as in the original work on the AA-IIR method [4], where f_s denotes the base sampling rate. For comparison purposes, a continuous-time antialiasing filter in the AA-IIR method is chosen to match this decimation filter. Causal spline interpolation in the Petrinović formulation (with a look-ahead $L = 6$) is chosen for the cubic interpolation kernel. The input signal amplitude is set at 10, and the base sampling rate is 44.1 kHz.

5.2.1. Numerical Integration

Firstly, we need to define a suitable numerical integration method for cubic AA-IIR. For the integral approximation, e.g. in equation (4), consider a quadrature formula with nodes t_i and weights w_i

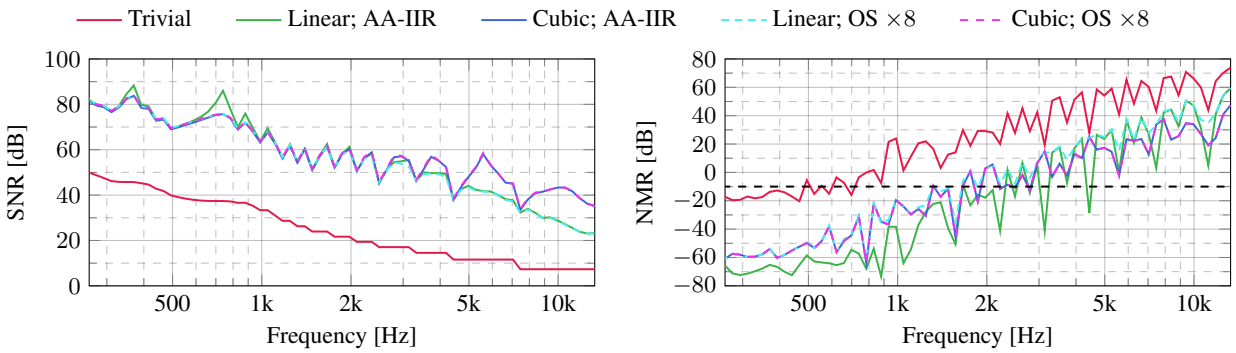

(a) SNR for OS and AA-IIR.

(b) NMR for OS and AA-IIR.

Figure 5: *Hard clipper simulation.*

over an unit interval $[0, 1]$ which results in the following expression for the AA-IIR output $y[n]$:

$$y[n] \approx e^{\alpha} y[n-1] + \sum_i A w_i e^{\alpha(1-t_i)} f(\widetilde{x}(n-1+t_i)),$$

where coefficients in front of nonlinear function values can be precomputed for each pole of the implemented antialiasing filter to lower computational cost.

Since there are no assumptions that we can make about the integrated expression, we can utilise the most general integration approaches such as composite midpoint and composite trapezoidal quadratures. The number of nodes in a composite quadrature scales as an oversampling factor, thus we can use $M = 8$ nodes for a fair comparison with oversampling. For the hard clipper, we consider the composite midpoint quadrature with nodes $t_i = \frac{2i-1}{2M}$ and weights $w_i = \frac{1}{M}$ for $i = 1, \ldots, M$.

5.2.2. *Comparison to Oversampling*

The linear AA-IIR method can be solved analytically for the hard clipper [4]. Because of this, linear AA-IIR significantly improves NMR by around 20 dB for virtually all inputs below 2 kHz compared to linear oversampling (see fig. 5b), but for the most part both methods stay below the audibility threshold. For higher frequencies, linear AA-IIR shows significant improvements in NMR for individual inputs corresponding to the situations where the largest aliased components are grouped around main harmonics and masked by them.

Compared with linear AA-IIR, cubic AA-IIR shows significant improvements in SNR up to 16 dB after 2.5 kHz (see fig. 5a). Dips in SNR for cubic AA-IIR (e.g. 7458 Hz) correspond to situations when a harmonic falls slightly over the Nyquist limit where the cubic interpolation kernel provides insufficient attenuation (see fig. 2b) thus creating a large aliased component. For lower frequencies, linear AA-IIR still has lower NMR values as numerical approximation in cubic AA-IIR counteracts the improved stopband attenuation of cubic interpolation. However, cubic AA-IIR also remains below the audibility threshold.

In addition, we see that the performance of cubic AA-IIR and cubic oversampling is virtually identical. This is significant, because the cubic AA-IIR method is more computationally efficient for oversampling factors $M \geq 3$ and a chosen antialiasing filter order $K = 8$ (see fig. 6) in terms of floating point operations (additions and multiplications combined). Moreover, for oversampling factors $M \geq 6$ cubic AA-IIR is more efficient than linear oversampling. For linear AA-IIR, operation count is dependant on a chosen approximation of the exponential function and the input signal, but on average it is cheaper compared to other methods [4].

It was also noted that IIR filtering though midpoint approximation of continuous-time convolution in AA-IIR requires fewer floating point operations compared with digital IIR filter in oversampling when $M \geq 3$ is chosen:

$$\forall K \in \mathbb{N}; M \in \mathbb{N}, M \geq 3 :$$
$$\underbrace{(4M+7)\lfloor \tfrac{K}{2} \rfloor + 2(M+1)K[2] - 1}_{\substack{\text{Operation count for midpoint approx.} \\ \text{of continuous-time convolution}}} < \underbrace{(3K + \lceil \tfrac{K+1}{2} \rceil)M}_{\substack{\text{Operation count for} \\ \text{digital IIR}}},$$

where $K[2] \coloneqq K \bmod 2$, $\lfloor \cdot \rfloor$ and $\lceil \cdot \rceil$ are floor and ceiling functions, respectively.

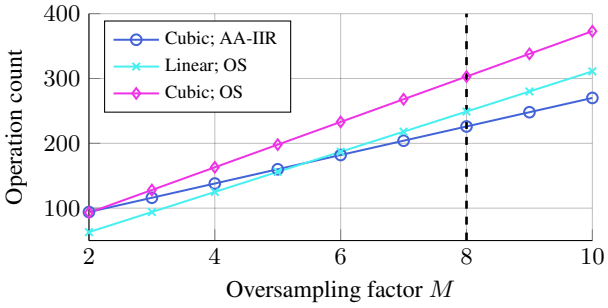

Figure 6: *Operation count for OS and AA-IIR (with composite midpoint integration) for an antialiasing filter order $K = 8$.*

5.3. Diode Clipper

For a stateful system, we first consider the diode clipper circuit (see fig. 8) which is a common test problem for antialiasing methods [5, 7, 8]. This circuit includes diodes as nonlinear elements, and can be fully described by the following differential equation [7]:

$$\frac{dv}{dt} = \frac{1}{C}\left[\frac{u-v}{R} - 2I_s \sinh\left(\frac{v}{N_i V_t}\right)\right], \tag{10}$$

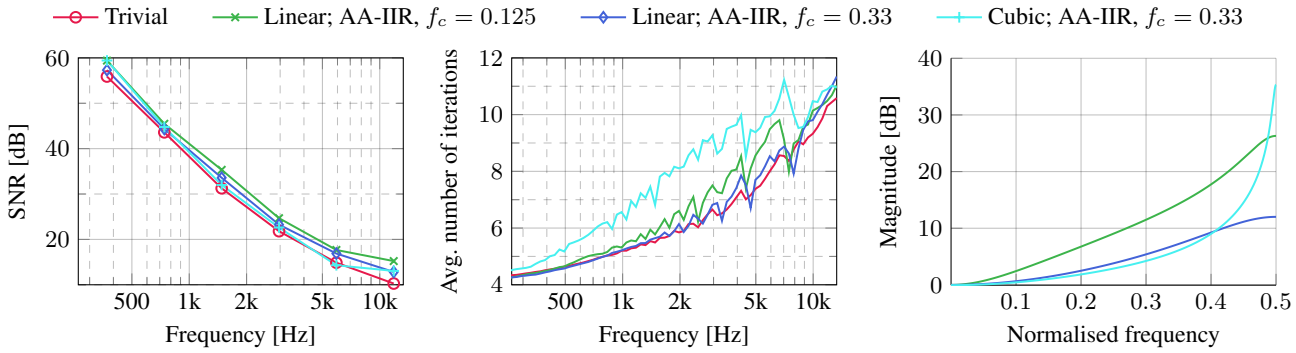

(a) Octave-averaged SNR.

(b) Newton-Raphson iterations.

(c) Compensation filters for AA-IIR.

Figure 7: *Diode clipper simulation.*

where u and v are input and output voltage, respectively, and component values are the resistance $R = 1$ kΩ, capacitance $C = 33$ nF, saturation current $I_s = 2.52$ nA, thermal voltage $V_t = 25.83$ mV and diode ideality factor $N_i = 1.752$.

In contrast with the study by La Pastina et al. [8], we apply the AA-IIR method with compensation filter directly to the embedded nonlinearity $\sinh(\cdot)$. For linear interpolation, an analytical solution to the AA-IIR method is available, while for cubic interpolation, the composite trapezoidal quadrature with $M = 8$ nodes is used. We discretise (10) with the trapezoidal rule, making use of the antialiased nonlinearity samples. The damped Newton-Raphson method is applied to the resulting circuit discretisation with 10^{-12} and 10^{-14} relative and absolute tolerance, respectively, 50 maximum iterations and 5 maximum subiterations. The input signal amplitude is set at 10 V, and the base sampling rate is 44.1 kHz.

Based on the stability analysis in Section 4.2.2, it is possible to employ a second-order Butterworth filter for linear AA-IIR. However, due to the high frequency peak in the compensation filter reaching 33.31 dB, the linear AA-IIR method has significantly worse antialiasing performance compared with the trivial implementation at the base sampling rate, with NMR rising by 7.8 dB at an input frequency of 987.77 Hz (see table 4).

Table 4: *SNR and NMR for linear AA-IIR with a second-order Butterworth filter ($f_c = 0.52$) on 10 V, 987.77 Hz input.*

Method	SNR	NMR
Trivial	40.62	14.88
Linear AA-IIR	38.70	22.68

This leaves us with a first-order Butterworth filter for linear and cubic AA-IIR. Chosen normalised cutoffs are $f_c = 0.125$ as in [8] and $f_c = 0.33$ which is a minimum possible cutoff for cubic interpolation. It should be noted that numerical integration relaxes cutoff restriction for cubic interpolation by an insignificant margin.

Compared to the trivial implementation, linear AA-IIR improves SNR by 2–5 dB (see fig. 7a). The filter with lower cutoff $f_c = 0.125$ is preferable. Cubic interpolation is inferior to linear interpolation with the same antialiasing filter. Similarly to the case of a second-order Butterworth filter, this is due to the large peak in the compensation filter compared to formulations employing linear interpolation (see fig. 7c). Overall, the AA-IIR method shows incomparable performance to oversampling by 2, which can improve SNR by up to 20 dB across the whole frequency spectrum [7, 16].

The peak of the compensation filter also correlates to the average number of iterations required in order to solve the nonlinear equation using the Newton-Raphson method. In fig. 7b we see that cubic AA-IIR requires the most iterations by a large margin, followed by linear AA-IIR with $f_c = 0.125$ which has a higher compensation peak than for $f_c = 0.33$. All of the AA-IIR methods generally require more iterations than trivial implementation. This correlation is due to the larger high frequency ripples in the waveform imposed by the compensation filter.

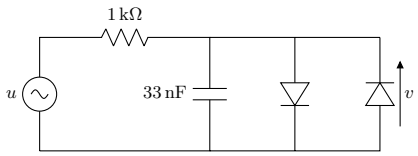

Figure 8: *Circuit diagram of the modelled diode clipper.*

5.4. Tube Screamer

For a further evaluation, we consider the clipping stage of the Tube Screamer overdrive pedal. Once again, clipping is achieved by diodes embedded in the system, but in an asymmetric arrangement. For full circuit diagrams, component values and state-space model the reader can refer to [7].

Due to the more prominent distortion compared with the diode clipper, we employ coupling of linear AA-IIR with oversampling by 2. Cubic AA-IIR is not considered due to its inferior performance. The trapezoidal rule is used for discretisation in combination with the capped Newton-Raphson method [18]. The input signal amplitude is set at 1 V, and the base sampling rate is 44.1 kHz.

In the spectrum plot for linear AA-IIR (see fig. 9b) we see that smaller aliased components, which correspond to frequencies far beyond the Nyquist limit, are attenuated significantly compared with plain oversampling (see fig. 9a). Nonetheless, the main aliased components around −60 dB in magnitude stay on the same level or are even amplified. Because of that, metrics do not change significantly and there is no perceptual difference between algorithms when tested on a sine sweep input signal.

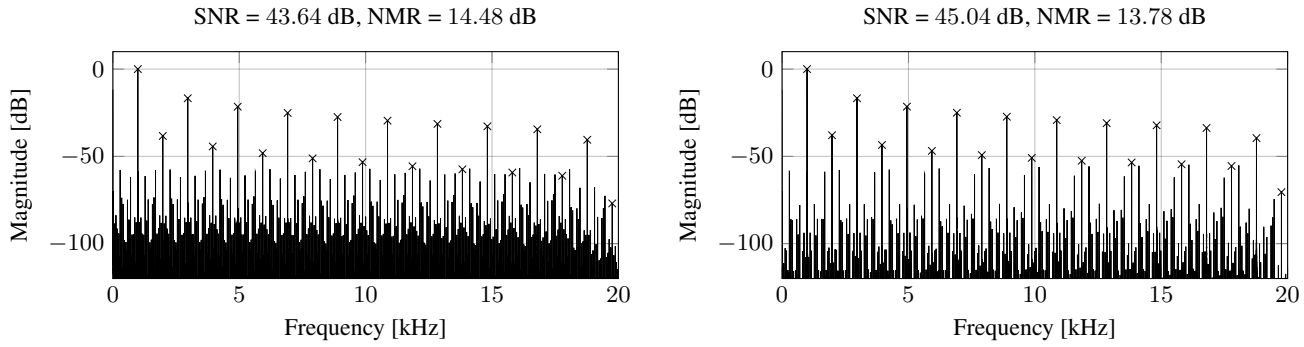

(a) Linear; OS ×2.

(b) Linear; OS ×2; AA-IIR, $f_c = 0.33$.

Figure 9: *Tube Screamer output spectrum for input at* 1 *V and* 987.77 *Hz (crosses indicate desired components).*

6. CONCLUSIONS

This paper has considered the application of cubic interpolation methods for antiderivative antialiasing in memoryless nonlinearities and stateful systems. MATLAB implementations of linear and cubic AA-IIR in hard clipper and diode clipper are available in the accompanying GitHub repository[1].

For memoryless nonlinearities, cubic interpolation showed improvements in aliasing reduction compared to linear interpolation for input signals with frequencies higher than 2.5 kHz. Implementation of cubic interpolation in AA-IIR formulation is preferable to oversampling due to the reduction in the floating point operation count, while preserving identical aliasing reduction. Further work is required to perceptually evaluate these improvements.

For stateful systems, application of interpolation kernels other than linear interpolation did not result in practically useful algorithms. Cubic interpolation imposes more severe restrictions on the antialiasing filter in order to maintain stability of the compensation filter compared with linear interpolation. Because of this, linear interpolation with a first order filter remains the only reasonable choice for the AA-IIR method. For considered case studies this combination showed insignificant improvements in aliasing reduction.

7. REFERENCES

[1] J. Kahles, F. Esqueda, and V. Välimäki, "Oversampling for Nonlinear Waveshaping: Choosing the Right Filters," *J. Audio Eng. Soc*, vol. 67, no. 6, pp. 440–449, 2019.

[2] S. Bilbao, F. Esqueda, J. Parker, and V. Välimäki, "Antiderivative Antialiasing for Memoryless Nonlinearities," *IEEE Signal Process. Lett.*, vol. 24, no. 7, pp. 1049–1053, 2017.

[3] J. Parker, V. Zavalishin, and E. Le Bivic, "Reducing the Aliasing of Nonlinear Waveshaping using Continuous-Time Convolution," in *Proc. Int. Conf. Digital Audio Effects*, 2016, pp. 137–144.

[4] P. P. La Pastina, S. D'Angelo, and L. Gabrielli, "Arbitrary-Order IIR Antiderivative Antialiasing," in *Proc. Int. Conf. Digital Audio Effects*, 2021, pp. 9–16.

[1] `https://github.com/victorzheleznov/dafx24`

[5] M. Holters, "Antiderivative Antialiasing for Stateful Systems," *Appl. Sci.*, vol. 10, no. 1, 2020.

[6] D. Albertini, A. Bernardini, and A. Sarti, "Antiderivative Antialiasing Techniques in Nonlinear Wave Digital Structures," *J. Audio Eng. Soc.*, vol. 69, pp. 448–464, 2021.

[7] A. Carson, "Aliasing Reduction in Virtual Analogue Modelling," M.S. thesis, University of Edinburgh, 2020.

[8] P. P. La Pastina and S. D'Angelo, "Antiderivative Antialiasing with Frequency Compensation for Stateful Systems," in *Proc. Int. Conf. Digital Audio Effects*, 2022, pp. 40–47.

[9] P. Thévenaz, T. Blu, and M. Unser, "Interpolation revisited," *IEEE Trans. Medical Imaging*, vol. 19, no. 7, pp. 739–758, 2000.

[10] D. Petrinović, "Continuous Time Domain Properties of Causal Cubic Splines," *Signal Process.*, vol. 89, pp. 1941–1958, 2009.

[11] D. Petrinović, "Causal Cubic Splines: Formulations, Interpolation Properties and Implementations," *IEEE Trans. Signal Process.*, vol. 56, pp. 5442–5453, 2008.

[12] C. de Boor, *A Practical Guide to Spline*, Springer, 1978.

[13] M. Unser, "Splines: a Perfect Fit for Signal and Image Processing," *IEEE Signal Process. Mag.*, vol. 16, no. 6, pp. 22–38, 1999.

[14] G. Meinsma and L. Mirkin, "L^2 Sampled Signal Reconstruction with Causality Constraints — Part I: Setup and Solutions," *IEEE Trans. Signal Process.*, vol. 60, no. 5, pp. 2260–2272, 2012.

[15] G. Meinsma and L. Mirkin, "L^2 Sampled Signal Reconstruction with Causality Constraints — Part II: Theory," *IEEE Trans. Signal Process.*, vol. 60, pp. 2273–2285, 2012.

[16] V. Zheleznov, "Interpolation Filters for Antiderivative Antialiasing," M.S. thesis, University of Edinburgh, 2023.

[17] P. Kabal, "An Examination and Interpretation of ITU-R BS.1387: Perceptual Evaluation of Audio Quality," Tech. Rep., McGill University, 2003.

[18] B. Holmes and M. van Walstijn, "Improving the Robustness of the Iterative Solver in State-Space Modelling of Guitar Distortion Circuitry," in *Proc. Int. Conf. Digital Audio Effects*, 2015.